Finite-Size Scaling Behaviors of Eigen Microstates near the Critical Point

Gaoke Hu[1,2,3], Jia-Qi Dong[4], Yongwen Zhang[5], Teng Liu[3,6], Wen-Long You[1,2], Maoxin Liu[3], and Xiaosong Chen[3,7*]

[1]*College of Physics, Nanjing University of Aeronautics and Astronautics, Nanjing 211106, China*
[2]*Key Laboratory of Aerospace Information Materials and Physics (NUAA), MIIT, Nanjing 211106, China*
[3]*School of Systems Science/Institute of Nonequilibrium Systems, Beijing Normal University, Beijing 100875, China*
[4]*Lanzhou Center for Theoretical Physics and Key Laboratory of Theoretical Physics of Gansu Province, Lanzhou University, Lanzhou 730000, China*
[5]*Data Science Research Center, Faculty of Science, Kunming University of Science and Technology, Kunming 650500, China*
[6]*Earth System Modelling, School of Engineering and Design, Technical University of Munich, Munich 85748, Germany*
[7]*Institute for Advanced Study in Physics and School of Physics, Zhejiang University, Hangzhou 310058, China*

(Received 19 August 2025; accepted manuscript online 11 December 2025)

In the eigen microstate approach (EMA), phase emergence is signaled by the condensation of an eigen microstate with a finite eigenvalue. The associated eigenvalue acts as an order parameter, exhibiting finite-size scaling (FSS) behaviors within the critical regime. The eigen microstate derived from EMA precisely characterizes the spatial structure of the emergent phase, which remains less explored in systems lacking translational invariance. Here, we propose an FSS form for the eigen microstate itself and numerically validate it using the two-dimensional Ising model under various boundary conditions. This result enables the derivation of FSS relations for correlation functions, which we verify through numerical simulations. Our results complete the FSS formalism for the EMA.

DOI: 10.1088/0256-307X/43/2/020001 CSTR: 32039.14.0256-307X.43.2.020001

1. Introduction. Phase transitions and critical phenomena are among the most extensively studied fields in statistical physics,[1–7] highlighting the profound role of scaling, universality, and renormalization in understanding emergent behaviors.[8–13] In recent decades, these foundational concepts have been extended to complex systems, spanning climate systems,[14] biological processes,[15,16] and social dynamics,[17,18] where collective behaviors arise from interactions among elementary units.[19–21] However, applying classical phase transition theory to complex systems remains challenging. For many real-world systems, computing free energy and analyzing singularities to probe criticality is often infeasible. Additionally, the diversity of phases in complex systems hinders a priori identification of order parameters.[22,23] Recent advances in machine learning, particularly neural networks, offer promising tools for detecting phase transitions.[24–28] Yet, these approaches face limitations, including low interpretability, imprecise determination of critical points and exponents, and a lack of robust frameworks to elucidate the collective mechanisms underlying transitions.

To address these challenges, we present the eigen microstate approach (EMA),[29–31] a framework for analyzing the emergent behaviors in complex systems. In EMA, a normalized ensemble matrix is constructed from experimental or simulated microstate samples, which is then decomposed into a complete set of orthogonal eigen microstates. These eigen microstates hierarchically capture collective behaviors across different scales, with their statistical significance quantified by the corresponding eigenvalues. EMA has been applied to diverse critical phenomena, encompassing discontinuous, and continuous transitions in the Vicsek model,[32] superradiant quantum phase transitions in Rabi systems,[33] Kármán vortex street dynamics in turbulent flows,[34] and systems exhibiting self-organized criticality.[35] Its capacity to identify dominant collective modes has been extended to real-world complex systems, including ecosystem dynamics[36] and climate systems.[37–39] For sea surface temperature data, EMA enhances the prediction accuracy of extreme climate events,[38] showcasing its potential for addressing practical challenges in complex systems.

In EMA, phase transitions are identified by the condensation of an eigen microstate, marked by a transition of its eigenvalue from zero to a finite value in the thermodynamic limit. The condensed eigen microstate characterizes the ordered phase, and its eigenvalue serves as an order parameter. Both quantities are derived directly from raw microstate data without manual feature engineering. Although previous studies have systematically established scaling properties for eigenvalues,[29–31] the scaling behaviors of eigen microstates, which are essential for capturing

*Corresponding author. Email: chenxs@bnu.edu.cn
© 2026 Chinese Physical Society and IOP Publishing Ltd. All rights, including for text and data mining, AI training, and similar technologies, are reserved.

the spatial structure of collective modes, remain unexplored. In this Letter, we bridge this gap by proposing a universal scaling formalism for eigen microstates, thereby refining the EMA framework.

2. Finite-Size Scaling of Eigen Microstates. For an N-component system, the microstate at time τ is described by an N-dimensional column vector $\boldsymbol{s}(\tau) = [s_1(\tau), s_2(\tau), \ldots, s_N(\tau)]^{\mathrm{T}}$, where $s_i(\tau)$ denotes the state of the i-th site. Given M total microstates, the $N \times M$ ensemble matrix $\boldsymbol{S}$ is constructed by normalizing each element as $\boldsymbol{S}_{i\tau} = s_i(\tau)/\sqrt{C_0}$, where $C_0 = \sum_{i=1}^{N}\sum_{\tau=1}^{M} s_i^2(\tau)$. Using singular value decomposition, $\boldsymbol{S}$ can be decomposed as $\boldsymbol{S} = \boldsymbol{U}\boldsymbol{\Sigma}\boldsymbol{V}^{\mathrm{T}}$. Here, $\boldsymbol{U} = [\boldsymbol{u}_1, \boldsymbol{u}_2, \ldots, \boldsymbol{u}_N]$ is an $N \times N$ unitary matrix, $\boldsymbol{V} = [\boldsymbol{v}_1, \boldsymbol{v}_2, \ldots, \boldsymbol{v}_M]$ is an $M \times M$ unitary matrix, and $\boldsymbol{\Sigma}$ is an $N \times M$ diagonal matrix with singular values $\sigma_1 \geqslant \sigma_2 \geqslant \cdots \geqslant \sigma_r \geqslant 0$ on the diagonal and zeros elsewhere,[40] where $r = \min(N, M)$. Each column of $\boldsymbol{U}$, such as $\boldsymbol{u}_I = [u_{1I}, u_{2I}, \ldots, u_{NI}]^{\mathrm{T}}$, is an eigenvector of the correlation matrix $\boldsymbol{S}\boldsymbol{S}^{\mathrm{T}}$. These eigenvectors define the eigen microstates, which represent the system's collective modes, while σ_I^2 quantifies the statistical weight (or probability) of $\boldsymbol{u}_I$.[29,30]

A phase transition manifests as the condensation of an eigen microstate, where its associated eigenvalue undergoes a zero-to-nonzero transition and serves as the order parameter. In the critical regime of a lattice system with linear size L, the dominant eigenvalue σ_I exhibits finite-size scaling (FSS) behavior,[29–31]

$$\sigma_I(t, L) = L^{-\beta/\nu} f_I(tL^{1/\nu}), \tag{1}$$

where f_I denotes the scaling function, $t \equiv (T - T_{\mathrm{c}})/T_{\mathrm{c}}$ the reduced temperature (T_{c} being the critical temperature), and β, ν represent critical exponents for the order parameter and correlation length, respectively.[29,30] We establish that this FSS form holds universally across boundary conditions, as demonstrated subsequently.

With the spatial position of component j denoted by $\boldsymbol{r}_j$, the eigen microstate $\boldsymbol{u}_I$ is represented as a spatial function $u_I(t, L, \boldsymbol{r}_j) \equiv u_{jI}$. In the critical regime, the correlation length ξ becomes comparable to the system size L. We propose that the spatial distribution of $\boldsymbol{u}_I$ obeys the FSS form,

$$u_I(t, L, \boldsymbol{r}_j) = L^{-d/2} P_I\Big(tL^{1/\nu}, \frac{\boldsymbol{r}_j}{L}\Big), \tag{2}$$

where P_I is a scaling function dependent on boundary conditions, and the factor $L^{-d/2}$ ensures normalization of $\boldsymbol{u}_I$ over the L^d-sized lattice. It is important to mention that deviations from the FSS form arise in small systems due to the influence of finite-size corrections.[7,41,42] For sufficiently large system sizes, these deviations become negligible.

3. Finite-Size Scaling of Correlation Function. While prior studies have established the FSS form of correlation functions under periodic boundary conditions,[43–49] their generalization to non-periodic boundaries remains an open question. We address this gap by deriving the FSS form of the correlation function through the scaling behavior of eigen microstates.

The correlation function, which quantifies statistical relationships between microscopic states at positions $\boldsymbol{r}_i$ and $\boldsymbol{r}_j$, is defined as

$$g(t, L, \boldsymbol{r}_i, \boldsymbol{r}_j) \equiv \frac{1}{M}\sum_{\tau=1}^{M} s_i(\tau) s_j(\tau). \tag{3}$$

Within the EMA framework, this function decomposes into a weighted superposition,

$$g(t, L, \boldsymbol{r}_i, \boldsymbol{r}_j) = \frac{C_0}{M}\sum_I \sigma_I^2 u_I(t, L, \boldsymbol{r}_i) u_I(t, L, \boldsymbol{r}_j), \tag{4}$$

where $C_0 \propto NM$ is a normalization factor. Combining the eigenvalue scaling [Eq. (1)] and eigen microstate scaling [Eq. (2)], we obtain the FSS ansatz,

$$g(t, L, \boldsymbol{r}_i, \boldsymbol{r}_j) = L^{-2\beta/\nu} G\Big(tL^{1/\nu}, \frac{\boldsymbol{r}_i}{L}, \frac{\boldsymbol{r}_j}{L}\Big), \tag{5}$$

where $G(x, \boldsymbol{r}, \boldsymbol{r}')$ is the scaling function. We can rewrite it in another form

$$g(t, L, \boldsymbol{r}_i, \boldsymbol{r}_j) = |\boldsymbol{r}_i - \boldsymbol{r}_j|^{-2\beta/\nu} G'\Big(tL^{1/\nu}, \frac{\boldsymbol{r}_i}{L}, \frac{\boldsymbol{r}_j}{L}\Big), \tag{6}$$

where $G'(x, \boldsymbol{r}, \boldsymbol{r}') = (|\boldsymbol{r} - \boldsymbol{r}'|/L)^{2\beta/\nu} G(x, \boldsymbol{r}, \boldsymbol{r}')$ is a scaling function. At the critical point, the bulk correlation function behaves as $g(t = 0, L \to \infty, \boldsymbol{r}_i, \boldsymbol{r}_j) \propto |\boldsymbol{r}_i - \boldsymbol{r}_j|^{-(d-2+\eta)}$. Comparing with the FSS form of the correlation function, we recover the standard scaling relation $2\beta/\nu = d - 2 + \eta$, which is well-established. For periodic boundaries, translational invariance implies that $G(x, \boldsymbol{r}_i, \boldsymbol{r}_j)$ depends only on $\boldsymbol{r}_i - \boldsymbol{r}_j$, in agreement with Ref. [49]. Besides the correlation function in Eq. (3), we note that connected correlation functions are also widely applied.[50–52] In the Supplementary Materials (SM), our numerical results confirm that the connected correlation function exhibits a similar FSS behavior.

4. Numerical Validation of the Finite-Size Scaling Relations. The Ising model has played a central role in studying phase transitions and critical phenomena.[53–56] Given its significance and rich behavior, we examine two-dimensional (2D) Ising models under different boundary conditions to validate the proposed FSS form of eigen microstates. Under periodic boundaries, the condensed eigen microstate corresponds to a uniform ferromagnetic phase,[29,30] trivially satisfying the eigen microstate scaling relation [Eq. (2)]. Below, we verify the scaling relations for eigenvalues, eigen microstates, and correlation functions under free and fixed boundary conditions.

The Hamiltonian of the Ising model is given by $H = -J\sum_{\langle i,j\rangle} s_i s_j$, where J is the nearest-neighbor coupling strength, and spins s_i take values ± 1. Microstates are sampled via Monte Carlo simulations,[57] from which we construct the ensemble matrix $\boldsymbol{S}$ and calculate eigen microstates $\{\boldsymbol{u}_I\}$ along with their eigenvalues $\{\sigma_I\}$. Temperature is measured in units of J/k_{B}, and k_{B} is the Boltzmann constant. The simulations are performed using the Wolff algorithm.[57] We begin each simulation with all spins aligned. The initial 20,000 microstates are discarded

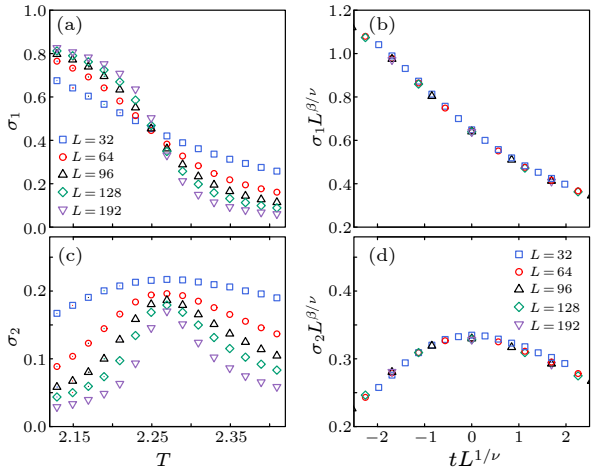

Fig. 1. Two largest eigenvalues (σ_1 and σ_2) of the two-dimensional (2D) Ising model under free boundary conditions. (a) Temperature dependence of the largest eigenvalue σ_1 for different system sizes. (b) FSS of σ_1. (c) Temperature dependence of the second-largest eigenvalue σ_2 across varying system sizes. (d) FSS of σ_2. Temperature is expressed in units of $J/k_{\rm B}$, where $k_{\rm B}$ is the Boltzmann constant. Error bars are smaller than the marker sizes.

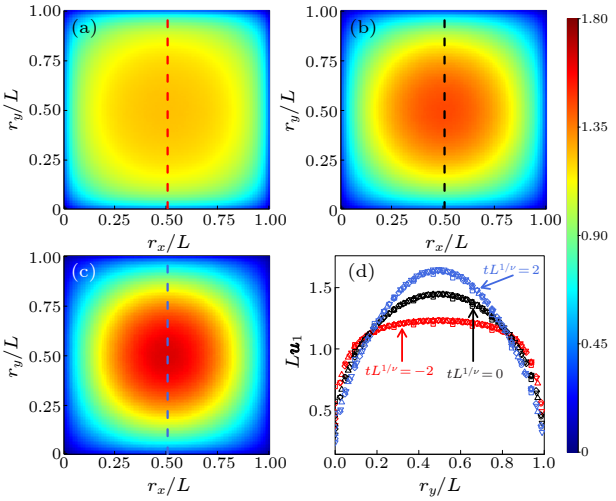

Fig. 2. Spatial distributions of the largest eigen microstate $\boldsymbol{u}_1$ in the 2D Ising model under free boundary conditions, shown at three scaled reduced temperatures: (a) $tL^{1/\nu} = -2$, (b) $tL^{1/\nu} = 0$, and (c) $tL^{1/\nu} = 2$ with a system size $L = 128$. (d) The scaling function of $\boldsymbol{u}_1$ collapses along the line at $L/2$ away from the boundary in the y-axis direction across different system sizes: $L = 32$ (□), 64 (◯), 96 (△), 128 (◇), and 192 (▽), with scaled reduced temperatures $tL^{1/\nu} = -2$ (red), 0 (black), and 2 (blue). Error bars are smaller than the marker sizes.

to allow the system to reach equilibrium. After equilibration, $M = 2 \times 10^6$ microstates are collected at each temperature, with a sampling interval of 200 Monte Carlo steps to ensure statistical independence. The use of millions of microstates ensures the convergence of eigenvalues and eigen microstates, with statistical errors on the order of 10^{-4}. While the required sample size for convergence is related to the sampling interval, this dependence is negligible for the large sample size employed in our study. Details can be found in the SM. Under free boundary conditions, no constraints are imposed at the boundaries. Under fixed boundary conditions, all spins located at boundaries are set to $s_i = 1$. In both cases, the ferromagnetic phase transition in Ising model is characterized by the condensation of the largest eigen microstates $\boldsymbol{u}_1$, with its associated eigenvalue σ_1 serving as the order parameter. Further details can be found in the SM.

We confirm the FSS behaviors of eigenvalues σ_I [Eq. (1)] under free boundary conditions. The largest and second-largest eigenvalues as functions of temperature T for various system sizes L are plotted in Figs. 1(a) and 1(c). The FSS functions of $\sigma_I L^{\beta/\nu}$ with respect to the scaling variable $tL^{1/\nu}$ are plotted in Figs. 1(b) and 1(d). Arising from finite-size corrections, slight deviations from data collapse are visible in the smallest system size ($L = 32$). The remaining curves for different values of L collapse onto a single line, where the critical point $T_{\rm c} \simeq 2.269$ and the critical exponent $\beta/\nu = 1/8$ for the 2D Ising are used.[53,54] The critical point and critical exponents can be determined directly within the framework of EMA. Detailed results are provided in SM.

Free boundary conditions break translational invariance, giving rise to a spatially modulated ferromagnetic phase, which is characterized by the dominant eigen microstate $\boldsymbol{u}_1$. The temperature-dependent evolution of $\boldsymbol{u}_1$ is shown in Fig. 2. Due to fewer neighboring interactions, boundary spins experience weaker constraints and flip more freely, resulting in reduced magnetization at the boundaries. Consequently, the ferromagnetic phase exhibits a monotonic increase in local magnetization from the boundaries toward the system's center. At low temperatures, the magnetization profile remains relatively flat [Fig. 2(a)], but as temperature increases, the central peak sharpens, as seen in Figs. 2(b) and 2(c).

A key observation is that these spatially modulated ferromagnetic phases are a general feature of finite systems and are characterized by FSS relations. To verify the FSS relations for the eigen microstates in Eq. (2), we analyze the profiles of $\boldsymbol{u}_1$ along the y-axis at a distance $L/2$ from the boundaries, as indicated by the colored dashed lines in Figs. 2(a)–2(c). The collapses of the FSS function for $\boldsymbol{u}_1$ at scaled reduced temperatures $tL^{1/\nu} = -2$, 0, and 2 are shown in Fig. 2(d). While slight deviations are visible for the smallest size ($L = 32$), no distinguishable deviations exist for larger systems. Besides $\boldsymbol{u}_1$, subsequent eigen microstates (i.e., $\boldsymbol{u}_2$ and $\boldsymbol{u}_3$) also adhere to the FSS relations, as demonstrated numerically in the SM. Since the FSS function of an eigen microstate at a fixed $tL^{1/\nu}$ depends only on the rescaled position $\boldsymbol{r}/L$, these spatial structures remain well-defined in the thermodynamic limit.

The FSS relations for both eigenvalues and eigen microstates are also confirmed under fixed boundary conditions. The largest eigenvalue σ_1 acts as the order parameter and adheres to the FSS relations given in Eq. (1) (see the SM for details). The temperature-dependent spatial evolution of $\boldsymbol{u}_1$ is illustrated in Fig. 3.

Fixed boundary conditions alter the spatial structure of $\boldsymbol{u}_1$, enhancing local magnetization near the boundaries.

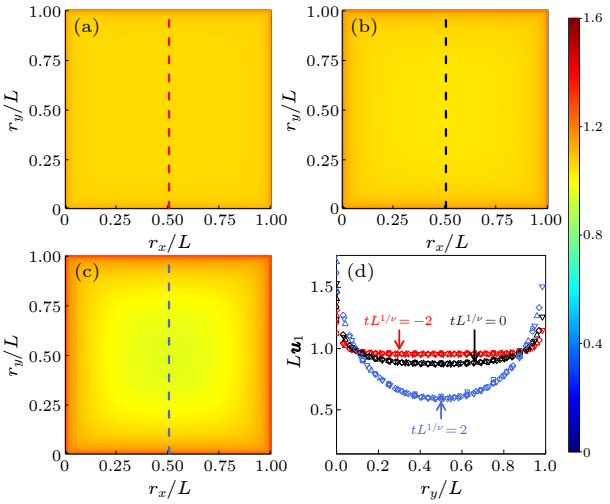

Fig. 3. Spatial distributions of the largest eigen microstates $\boldsymbol{u}_1$ in the 2D Ising model under fixed boundary conditions, displayed at three scaled reduced temperatures: (a) $tL^{1/\nu} = -2$, (b) $tL^{1/\nu} = 0$, and (c) $tL^{1/\nu} = 2$ with a system size $L = 128$. (d) The scaling function of $\boldsymbol{u}_1$ collapses along the line at $L/2$ away from the boundary in the y-axis direction across different system sizes: $L = 32$ (□), 64 (◯), 96 (△),128 (◊), and 192 (▽) at scaled reduced temperatures: $tL^{1/\nu} = -2$ (red), 0 (black), and 2 (blue). Error bars are smaller than the marker size.

At high temperatures [Fig. 3(c)], the magnetization profile decays steeply from the boundaries toward the system center. As temperature decreases, this profile gradually flattens [Figs. 3(a) and 3(b)]. These boundary-induced spatial modulations are consistent with the proposed FSS relations for eigen microstates, which are validated in Fig. 3(d). The profiles of $\boldsymbol{u}_1$ along the y-axis at a distance $L/2$ from the boundaries are plotted for fixed scaled temperatures $tL^{1/\nu} = -2, 0, 2$ across different system sizes. When rescaled by $\boldsymbol{r}/L$, the profiles of $L\boldsymbol{u}_1$ collapse onto a single curve, confirming the FSS prediction. Additional numerical validation for subsequent eigen microstates (i.e., $\boldsymbol{u}_2$, $\boldsymbol{u}_3$, and $\boldsymbol{u}_4$) is provided in the SM. Thus, the FSS ansatz for eigen microstates introduced in Eq. (2) is validated under fixed boundary conditions.

We further numerically verify the FSS relation for the correlation function [Eq. (5)] in the 2D Ising model under both free and fixed boundary conditions. Through Monte Carlo simulations, we calculate the two-point correlation function $g(t, L, \boldsymbol{r}_0, \boldsymbol{r})$, where one point's position $\boldsymbol{r}_0$ is fixed as a reference point. To confirm the FSS relation, we analyze the rescaled correlation function $L^{2\beta/\nu}g(t, L, \boldsymbol{r}_0, \boldsymbol{r})$ as a function of the rescaled distance $(\boldsymbol{r} - \boldsymbol{r}_0)/L$. Unlike the verification of the FSS form for eigenvalues and eigen microstates (Figs. 1–3), which requires the computationally expensive singular value decomposition of an ensemble matrix, the correlation function is calculated directly from its definition in Eq. (3). Thus, we can verify the FSS form of the correlation function in much larger systems in Fig. 4.

For free boundary conditions, we anchor the reference point $\boldsymbol{r}_0$ at the system center $(L/2, L/2)$. Figure 4(a) demonstrates the collapse of rescaled correlation functions

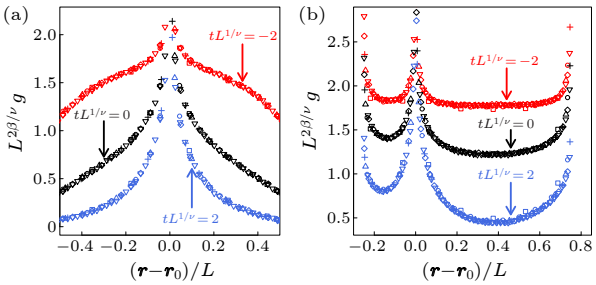

Fig. 4. FSS of correlation functions in the 2D Ising model. (a) Under free boundary conditions, the rescaled correlation function $L^{2\beta/\nu}g(t, L, \boldsymbol{r}_0, \boldsymbol{r})$ versus the scaled position $(\boldsymbol{r} - \boldsymbol{r}_0)/L$ along the x-axis (offset by $L/2$ from the boundary), with reference point $\boldsymbol{r}_0 = (L/2, L/2)$. (b) Corresponding results under fixed boundary conditions with reference point $\boldsymbol{r}_0 = (L/4, L/2)$. Data are for system sizes $L = 32$ (□), 64 (◯), 128 (△), 256 (+), 512 (◊), and 1024 (▽) at scaled temperatures $tL^{1/\nu} = -2$ (red), 0 (black), and 2 (blue). Error bars are smaller than marker sizes.

along the x-axis (offset by $L/2$ from the boundary) for scaled reduced temperatures $tL^{1/\nu} = -2$, 0, and 2 across system sizes $L = 32$ to 1024. Under fixed boundary conditions, similar scaling collapses are observed in Fig. 4(b), where the reference point is shifted to $\boldsymbol{r}_0 = (L/4, L/2)$. The influence of the finite-size corrections for smallest size $(L = 32)$ is visible in Fig. 4(b), and becomes negligible in larger system sizes. The collapse in both cases confirms the validity of the proposed FSS relation for the correlation function. Notably, figure 4 reveals distinct spatial profiles of $g(t, L, \boldsymbol{r}_0, \boldsymbol{r})$ under different boundary conditions, indicating that the scaling function G explicitly depends on boundary effects. Since G depends solely on the rescaled position $\boldsymbol{r}/L$, these boundary-induced differences in correlation functions persist in the thermodynamic limit.

5. Conclusions and Discussion. We investigate the FSS behaviors of eigen microstates, which are introduced to identify phase transitions and characterize collective modes in statistical ensembles. Using the EMA, we extract eigen microstates and their corresponding eigenvalues from system microstates, where the condensation of an eigen microstate signals the emergence of an ordered phase, with its eigenvalue defining the order parameter. We introduce FSS forms for dominant eigen microstates and their eigenvalues under different boundary conditions. These scaling relations demonstrate that in the critical regime, the spatial structure of eigen microstates is governed by two fundamental ratios: the relative correlation length ξ/L and the rescaled position $\boldsymbol{r}/L$, where ξ is the correlation length, L is the system size, and $\boldsymbol{r}$ represents spatial positions. From these FSS relations, we derive scaling behaviors for the correlation function across the entire system, providing broad applicability in studying critical phenomena. The proposed FSS relations for eigenvalues, eigen microstates, and correlation functions are numerically validated in the 2D Ising model under both free and fixed boundary conditions.

The application of the EMA to large systems requires singular value decomposition of the ensemble matrix, which can be computationally demanding. However,

since the physical behavior of a system is often captured by a small number of dominant eigen microstates, the Lanczos algorithm[58] offers an efficient alternative by computing these key modes without performing a full matrix decomposition, thereby significantly reducing computational requirements. In addition, we have developed a renormalization group theory for EMA,[31] which enables the extrapolation of system properties to larger scales. The computational cost of EMA is justified by its unique ability to directly extract collective modes from data, without manual feature selection or predefined order parameters, thereby offering a versatile framework for studying a wide range of systems.

In this work, we have focused on the FSS behaviors of eigen microstates in lattice systems around the continuous phase transition point. It would be meaningful to extend such analysis to more general systems, such as tree-graph structures or complex networks, where novel types of phase transitions may occur.[59,60] In future studies, we aim to systematically examine the applicability of the scaling relations established here, thereby providing a theoretical foundation for investigating real-world complex systems.

Acknowledgments. This work was supported by the National Natural Science Foundation of China (Grant Nos. 12405032, 12135003, and 11947231).

References

[1] Landau L D 1937 *Zh. Eksp. Teor. Fiz.* **11** 19
[2] Wilson K G and Fisher M E 1972 *Phys. Rev. Lett.* **28** 240
[3] Fisher M E and Barber M N 1972 *Phys. Rev. Lett.* **28** 1516
[4] Cardy J 1996 *Scaling and Renormalization in Statistical Physics* (Cambridge University Press)
[5] Hu G, Lü Z, Lin H, and Zheng H 2022 *Phys. Rev. A* **105** 043710
[6] Hu G, Lü Z, Lin H, and Zheng H 2023 *Phys. Rev. A* **108** 023723
[7] Privman V and Fisher M E 1984 *Phys. Rev. B* **30** 322
[8] Wilson K G 1983 *Rev. Mod. Phys.* **55** 583
[9] Stanley H E 1999 *Rev. Mod. Phys.* **71** S358
[10] Fisher M E 1998 *Rev. Mod. Phys.* **70** 653
[11] Barmatz M, Hahn I, Lipa J A, and Duncan R V 2007 *Rev. Mod. Phys.* **79** 1
[12] Gasparini F M, Kimball M O, Mooney K P, and Diaz-Avila M 2008 *Rev. Mod. Phys.* **80** 1009
[13] Perron J K, Kimball M O, Mooney K P, and Gasparini F M 2010 *Nat. Phys.* **6** 499
[14] Steffen W, Richardson K, Rockström J, Schellnhuber H J, Dube O P, Dutreuil S, Lenton T M, and Lubchenco J 2020 *Nat. Rev. Earth Environ.* **1** 54
[15] Brangwynne C P, Eckmann C R, Courson D S, Rybarska A, Hoege C, Gharakhani J, Jülicher F, and Hyman A A 2009 *Science* **324** 1729
[16] Muñoz M A 2018 *Rev. Mod. Phys.* **90** 031001
[17] Castellano C, Fortunato S, and Loreto V 2009 *Rev. Mod. Phys.* **81** 591
[18] Yakovenko V M and Rosser J B 2009 *Rev. Mod. Phys.* **81** 1703
[19] Dorogovtsev S N, Goltsev A V, and Mendes J F F 2008 *Rev. Mod. Phys.* **80** 1275
[20] Scheffer M, Bascompte J, Brock W A, Brovkin V, Carpenter S R, Dakos V, Held H, van Nes E H, Rietkerk M, and Sugihara G 2009 *Nature* **461** 53
[21] Baxter G J, Dorogovtsev S N, Goltsev A V, and Mendes J F F 2012 *Phys. Rev. Lett.* **109** 248701
[22] Hu J, Amor D R, Barbier M, Bunin G, and Gore J 2022 *Science* **378** 85
[23] Zheng Z, Xu C, Fan J, Liu M, and Chen X 2024 *Chaos* **34** 022101
[24] Carrasquilla J and Melko R G 2017 *Nat. Phys.* **13** 431
[25] van Nieuwenburg E P L, Liu Y H, and Huber S D 2017 *Nat. Phys.* **13** 435
[26] Reichstein M, Camps-Valls G, Stevens B, Jung M, Denzler J, Carvalhais N, and Prabhat 2019 *Nature* **566** 195
[27] Yin J, Pei Z, and Gao M C 2021 *Nat. Comput. Sci.* **1** 686
[28] Hu G K, Sun Y, Liu T, Zhang Y W, Liu M X, Fan J F, Chen W, and Chen X S 2023 *Sci. China-Phys. Mech. Astron.* **66** 120511
[29] Hu G K, Liu T, Liu M X, Chen W, and Chen X S 2019 *Sci. China-Phys. Mech. Astron.* **62** 990511
[30] Sun Y, Hu G K, Zhang Y W, Lu B, Lu Z H, Fan J F, Li X T, Deng Q, and Chen X S 2021 *Commun. Theor. Phys.* **73** 065603
[31] Liu T, Hu G K, Dong J Q, Fan J F, Liu M X, and Chen X S 2022 *Chin. Phys. Lett.* **39** 080503
[32] Li X, Xue T T, Sun Y, Fan J F, Li H, Liu M X, Han Z G, Di Z R, and Chen X S 2021 *Chin. Phys. B* **30** 128703
[33] Hu G K, Liu M X, and Chen X S 2023 *Physica A* **630** 129210
[34] Li X, Xiang X, Xue T, Wang L, and Chen X 2024 *Sci. China-Phys. Mech. Astron.* **67** 110511
[35] Zhang Y, Liu M, Hu G, Liu T, and Chen X S 2024 *Phys. Rev. E* **109** 044130
[36] Wang X, Fan H, Chen X, Xie Y, and Wang H 2024 *Ecol. Indic.* **159** 111689
[37] Chen X J, Ying N, Chen D, Zhang Y W, Lu B, Fan J F, and Chen X S 2021 *Chaos* **31** 071102
[38] Ma X, Liang R, Chen X, Xie F, Zuo J, Sun C, and Ding R 2024 *Geophys. Res. Lett.* **51** e2024GL110943
[39] Tu H, Wang S, Meng J, Zhang Y, Chen X, Chen D, and Fan J 2025 *Sci. China-Phys. Mech. Astron.* **68** 240511
[40] Klema V and Laub A 1980 *IEEE Trans. Automat. Contr.* **25** 164
[41] Binder K 1981 *Z. Phys. B* **43** 119
[42] Privman V 1990 *Finite Size Scaling and Numerical Simulation of Statistical Systems* (World Scientific)
[43] Brankov J G and Danchev D M 1991 *J. Math. Phys.* **32** 2543
[44] Kutlu B and Aktekin N 1995 *Physica A* **215** 370
[45] Chen X and Dohm V 2000 *Eur. Phys. J. B* **15** 283
[46] Bugrii A I and Lisovyy O O 2004 *Theor. Math. Phys.* **140** 987
[47] Tomita Y and Okabe Y 2002 *Phys. Rev. B* **66** 180401
[48] de Queiroz S L A and Stinchcombe R B 1999 *Phys. Rev. E* **60** 5191
[49] Zhang X, Hu G K, Zhang Y W, Li X T, and Chen X S 2018 *Sci. China-Phys. Mech. Astron.* **61** 120511
[50] Brézin E and Zee A 1994 *Phys. Rev. E* **49** 2588
[51] Tran M C, Garrison J R, Gong Z X, and Gorshkov A V 2017 *Phys. Rev. A* **96** 052334
[52] Grigera T S 2021 *J. Phys. Complex.* **2** 045016
[53] Onsager L 1944 *Phys. Rev.* **65** 117
[54] Yang C N 1952 *Phys. Rev.* **85** 808
[55] Binder K 1981 *Phys. Rev. Lett.* **47** 693
[56] Baxter R J 1982 *Exactly Solved Models in Statistical Mechanics* (Academic Press)
[57] Wolff U 1989 *Phys. Rev. Lett.* **62** 361
[58] Parlett B N and Scott D S 1979 *Math. Comput.* **33** 217
[59] Eggarter T P 1974 *Phys. Rev. B* **9** 2989
[60] Müller-Hartmann E and Zittartz J 1974 *Phys. Rev. Lett.* **33** 893